Localization of minodronate in mouse femora through isotope microscopy

Hiromi Hongo[1#], Muneteru Sasaki [1,2#], Sachio Kobayashi[3], Tomoka Hasegawa[1], Tomomaya Yamamoto[1], Kanako Tsuboi[1], Erika Tsuchiya[1], Tomoya Nagai[1], Naznin Khadiza[1], Miki Abe[1], Ai Kudo[1], Kimimitsu Oda[4], Paulo Henrique Luiz de Freitas[5], Minqi Li[6], Hisayoshi Yurimoto[3] and Norio Amizuka[1]

[1]Department of Developmental Biology of Hard Tissue, Graduate School of Dental Medicine, Hokkaido University, Sapporo, Japan, [2]Department of Applied Prosthodontics, Unit of Translational Medicine, Graduate School of Biomedical Sciences, Nagasaki University, Nagasaki, Japan, [3]Natural History Sciences, Isotope Imaging Laboratory, Creative Research Institution, Hokkaido University, Sapporo Japan, [4]Division of Biochemistry, Graduate School of Medical and Dental Sciences, Niigata University, Niigata, Japan, [5]Dental School, Federal University of Sergipe at Lagarto, Aracaju, Brazil, [6]Shandong Provincial Key Laboratory of Oral Biomedicine, The School of Stomatology, Shandong University, Jinan, China

Running title: ***Localization of minodronate in bone***

#These authors contributed equally to this study

Address for correspondence:

Norio Amizuka, DDS, PhD
Department of Developmental Biology of Hard Tissue
Graduate School of Dental Medicine, Hokkaido University
Kita 13 Nishi 7 Kita-ku
Sapporo, 060-8586, Japan
Tel: +81-11-706-4223
Fax: +81-11-706-4226
E-mail: amizuka@den.hokudai.ac.jp

Abstract

Minodronate is highlighted for its marked and sustained effects on osteoporotic bones. To determine the duration of minodronate's effects, we have assessed the localization of the drug in mouse bones through isotope microscopy, after labeling it with a stable nitrogen isotope (^{15}N-minodronate). In addition, minodronate-treated bones were assessed by histochemistry and TEM. Eight-weeks-old male ICR mice received ^{15}N-minodronate (1mg/kg) intravenously and were sacrificed after three hours, 24 hrs, one week and one month. Isotope microscopy showed that ^{15}N-minodronate was present mainly beneath osteoblasts rather than nearby osteoclasts. At 3 hrs after minodronate administration, histochemistry and TEM showed osteoclasts with well-developed ruffled borders. However, osteoclasts were roughly attached to the bone surfaces and did not feature ruffled borders at 24 hrs after minodronate administration. The numbers of TRAP-positive osteoclasts and ALP-reactive osteoblastic area were not reduced suddenly, and apoptotic osteoclasts appeared in 1 week and 1 month after the injections. Von Kossa staining demonstrated that osteoclasts treated with minodronate did not incorporate mineralized bone matrix. Taken together, minodronate accumulates in bone underneath osteoblasts rather than under bone-resorbing osteoclasts; therefore, it is likely that the minodronate-coated bone matrix is resistant to osteoclastic resorption, which results in a long-lasting and bone-preserving effect.

199 words

Key words: ***minodronate, osteoclast, osteoblast, isotope microscopy, bisphosphonate***

Introduction

Bisphosphonates are mainstream drugs for the treatment of osteoporosis. Drugs of this class have high affinity for crystalline calcium phosphates [1-3], thus binding to calcium phosphates in the bone matrix upon administration. When osteoclasts degrade bone tissue bound to bisphosphonates, bone resorption is inhibited as the drug induces osteoclast apoptosis [4, 5].

Among the several commercially available bisphosphonates, alendronate is the most commonly used one. In general, nitrogen-containing bisphosphonates (such as pamidronate, alendronate, ibandronate, zoledronate and risedronate) act by inhibiting farnesyl pyrophosphate synthase, an enzyme involved in the mevalonate pathway [6, 7], which then impairs protein prenylation, especially that of the small GTPase of the Ras family [8]. These small GTPase proteins are crucial for vesicular trafficking and cell survival and seem to be involved in the cytoskeletal organization of bone-resorbing osteoclasts [9-11]. In short, the cellular events that lead to osteoclastic inhibition seem to be shared by all nitrogen-containing bisphosphonates. On the other hand, bisphosphonate-driven osteoclastic inhibition appears to reduce osteoblastic population and bone formation, which can negatively affect bone turnover as demonstrated by decreased bone formation and mineral apposition rates in rats [12, 13], mice [14] and dogs [15].

Minodronate, a third-generation, nitrogen-containing bisphosphonate, is an approved drug for treatment of osteoporosis in the Japanese market [16-18]. Studies showed that minodronate suppressed bone resorption in ovariectomized rats and cynomolgus monkeys [19-21] and affected cortical bone response to mechanical loading in rats [22]. In addition, other *in vivo* and *in vitro* studies reported on the high potency of minodronate compared to alendronate regarding the inhibition of bone resorption [23], with an intermediate mineral-binding affinity [24].

Since patients seem to prefer weekly and monthly dosing regimens [25], long-acting bisphosphonates such as minodronate are gradually becoming the first line of treatment for many prescribing physicians. Still, a pervasive question among medical professionals and researchers is how can a single dose of bisphosphonate sustain its effects for over a month?

Therefore, we postulated that the localization of minodronate may offer new insights that might help address this issue. For instance, the use of radioisotope-labeled minodronate may assist on determining the localization and distribution of minodronate *in vivo*; however, animal studies involving radioisotopes are ethically questionable. We have explored the idea of using minodronate's own high affinity for binding crystalline calcium phosphates in the bone matrix to circumvent that limitation by substituting ^{15}N (very rare in nature) for ^{14}N (naturally abundant) in the minodronate molecule. ^{15}N-minodronate was then injected into mice to determine the localization of ^{15}N-minodronate through using isotope microscopy. Isotope microscopy is a mode of secondary ion mass spectrometry and two-dimensional isotope detection technique [26-28]. Recently, isotope microscope systems have been used to analyze living matter specimens [29].

To contribute for a better understanding on the mechanism of the sustained minodronate effects, we have examined the localization of ^{15}N-minodronate in murine bone through isotope microscopy complemented by histochemistry and transmission electron microscopy (TEM) observations.

Materials and methods

Preparation of ^{15}N- and ^{13}C-labelled minodronate

The ^{14}N and ^{12}C in the minodronate molecule were substituted with the stables isotopes ^{15}N and ^{13}C to generate {1-hydroxy-2-[(1-^{15}N)imidazo[1,2-a]pyridin-3-yl]($^{13}C2$)ethane-1,1-diyl}bis(phosphonic acid) hydrate **(Fig.1)**, which was kindly provided by Astellas Pharma Inc., Tokyo, Japan. The isotope microscope of the Creative Research Institution, Hokkaido University [26] was used for identification and localization of ^{15}N of ^{15}N- and ^{13}C-labelled minodronate. For the sake of convenience, ^{15}N- and ^{13}C-labelled minodronate will be referred to as ^{15}N-minodronate from here on.

Animals and tissue preparation

All animal experiments were approved by Hokkaido University and were conducted in accordance with the standards of humane animal care (No. 15-0030). Mice were anesthetized with an intraperitoneal injection of chloral hydrate, and then, were injected with ^{15}N-minodronate (1mg/kg) through the external jugular vein. Three hours, 24 hrs, 1 week and 1month after the injection, mice (n=6 for each) were perfused with 4% paraformaldehyde diluted in 0.1M phosphate buffer (pH 7.4, for histochemistry) or a mixture of 2% paraformaldehyde + 2.5% glutaraldehyde diluted in 0.067M cacodylate buffer (pH7.4, for isotope microscopy and transmission electron microscopy or TEM) through the heart's left ventricle. Femora were removed and immersed in the respective fixatives for 18 hurs (for histochemistry) or 3 days (for isotope microscopy and TEM) at 4 ^{o}C. Specimens for histochemistry were decalcified with 10% ethlenedimine tetraacedic disodium salt (EDTA-2Na) and dehydrated in ascending ethanol solutions prior to paraffin embedding. Samples for isotope microscopy were not decalcified, but instead immediately dehydrated, and then embedded in epoxy resin (Epon 812, Taab, Berkshine, UK). Some TEM specimens

were decalcified with 5% EDTA-2Na, but others were not decalcified. All TEM specimens were post-fixed with 1% osmium tetraoxide in 0.1M cacodylate buffer for 4 hrs at 4 ^{o}C, and dehydrated in ascending acetone solutions prior to embedding in epoxy resin. Semi-thin sections were placed on Si wafers for isotope microscope observation. Ultra-thin sections were stained with uranyl acetate and lead citrate for TEM observations (Hitachi H-7100 Hitachi Co. Ltd, Tokyo, Japan) at 80 kV.

Isotope microscopy

The sections placed on Si wafers were coated with a 30-nm layer of gold to prevent the accumulation of positive charges generated by the primary beam of the isotope microscopy. Hokkaido University's isotope microscope system (Cameca IMS 1270＋SCAPS) was used to visualize isotope distribution in the bone tissue, a technique known as isotopography [26, 27, 28, 29, 30].

Frequency histogram for osteoblast and osteoclast numbers and $^{15}N/^{14}N$ intensity ratio

To understand how much ^{15}N-minodronate was deposited beneath osteoblasts (bone forming surfaces) or osteoclasts (bone resorbing surfaces), we counted the osteoblasts and osteoclasts seen on bone surfaces labeled with ^{15}N-minodronate. Semi-thin sections of metaphyseal areas were used to generate data for the histogram. The intensity of ^{15}N (^{15}N-minodronate) lines seen underneath osteoblasts or osteoclasts was divided by the intensity of ^{14}N labeling in the same region. A series of $^{15}N/^{14}N$ ratios is shown on the horizontal axis of the histogram, while the vertical axis shows the numbers of osteoblasts or osteoclasts located on the bone surfaces with the corresponding $^{15}N/^{14}N$ ratio, thus indicating the volume of deposited ^{15}N-minodronate per surface type (bone forming vs. bone resorbing).

Double staining for tissue nonspecific alkaline phosphatase (ALP) and tartrate-resistant acid phosphatase (TRAP)

Dewaxed paraffin sections were treated for endogenous peroxidase inhibition with 0.3% hydrogen peroxide in phosphate buffered saline (PBS) for 20 min and for nonspecific staining blocking with 1% bovine serum albumin in PBS (1% BSA-PBS) for 30 min at room temperature (RT). Section were incubated with rabbit polyclonal antisera against tissue

nonspecific alkaline phosphatase (ALP) [31] for 2 hrs at RT, and then incubated with horseradish peroxidase-conjugated anti-rabbit IgG for 1 hr at RT. Immunoreactions were detected with 3.3'-diaminobenzidine tetrahydrochloride (Dojindo Laboratorise, Kumamoto, Japan). Following immunostaining, tartrate-resistant acid phosphatase (TRAP) was detected as previously described [32]. In short, slides were rinsed with PBS and incubated in a mixture of 2.5mg of naphthol AS-BI phosphate (Sigma-Aldrich, St. Louis, MO), 18mg of red violet LB (Sigma-Aldrich) salt, and 100mML (+) tartaric acid (0.76g) diluted in 30 ml of a 0.1M sodium acetate buffer (pH 5.0) for 15min at 37 ^{o}C.

Von Kossa staining

Undecalcified semi-thin section were incubated with an aqueous solution of 5% silver nitrate (Wako Pure Chemical Industries, Tokyo, Japan) for 60 min at RT under sunlight until taking on a dark brown color, as previously described [33] .

Statistical analyses for osteoclast number, osteoblastic area and percentage of apoptotic osteoclasts

Sagittal femora sections from samples of all time points (3 hrs, 24 hrs, 1 week and 1 month, n=6 for each) were cut as shown in **Fig. 2**. The region of interest (ROI) for counting TRAP-positive osteoclasts and measuring the area of ALP-reactive osteoblastic cells, as well as the determination of percentage of apoptotic osteoclasts was set as a boxed area neighboring the chondro-osseous junction and the endosteal surfaces of the cortical bone up to a horizontal line 2 mm distant from the chondro-osseous junction. As reported previously [33], ALP-positive cells located on bone surface were considered osteoblasts, while multinucleated (more than two nuclei) TRAP-reactive cells were regarded as osteoclasts. TRAP-positive osteoclasts with nuclear pyknosis were categorized as apoptotic osteoclasts. We counted the numbers of TRAP-positive osteoclasts and also measured the ALP-reactive area in the ROI by using the ImagePro Plus 6.2 software (Media Cybernetics, Silver Spring, MD). The percentage of apoptotic osteoclasts was obtained after dividing the number of pycknotic, TRAP-positive osteoclasts by the total osteoclast number.

Bone histomorphometry of BV/TV, Tb.N, Tb.Th and Tb.Sp

Bone histomorphometric static parameters were assessed as presented in a recent report from our group [34]. In brief, a 400µm x 600µm region of interest (ROI) located 150µm below the growth plate of the femoral metaphysis (n=6 for each) was used for assessing the following static parameters: bone volume/tissue volume (BV/TV), trabecular number (Tb.N), trabecular thickness (Tb.Th), trabecular separation (Tb.Sp). Whenever possible, abbreviations and calculations followed the guidelines of the ASBMR Histomorphometry Nomenclature Committee [35].

Statistical analysis

One-way ANOVA and the Tukey-Kramer multiple comparisons test were used to assess the presence of statistical differences among groups. All values are presented as mean ± standard deviation. The level of significance was set to $p < 0.01$.

Results

Histology of femoral metaphyseal trabeculae and TRAP/ALP double histochemistry after minodronate administration

Femora treated with minodronate showed time-from-administration-dependent increases in metaphyseal bone **(See Figs.2a-d and 2i-l)**. The histological observations demonstrated that trabeculae were more robust at 1 week and 1 month after minodronate administration than at 3 hrs and 24 hrs after the injections **(Fig. 2a-d)**. At higher magnification, osteocytes seemed intact, and no signs of inflammation or microdamage were identified at all time points **(Figs. 2e-h)**. Consistently, BV/TV at 1 week and 1 month after minodronate administration increased significantly when compared with that seen 3 hrs after the drug administration **(Fig.2i)**. Conversely, Tb.Sp. was significantly reduced at 1 week and 1 month after minodronate administration **(Fig. 2j)**. Despite the absence of statistical significance concerning Tb. Th **(Fig. 2i)**, there was significant increase in Tb.N 1 month after the administration when compared to values seen 3 hrs after the injections **(Fig. 2k)**.

At earlier time points (3 hrs and 24 hrs), the distribution of TRAP-positive osteoclasts and ALP-reactive osteoblasts was similar **(Figs. 3a, b, e** and **f)**, which is consistent with the absence of statistically significant differences in the number of osteoclasts and in ALP-reactive area **(Figs. 3i** and **j)**. Several TRAP-positive osteoclasts and ALP-reactive areas were seen at 1 week and 1 month post-injection despite the obvious increase in trabecular volume **(Figs. 3g-j)**. At higher magnification, apoptotic osteoclasts with nuclear pyknosis began to appear in 1 week and 1 month samples **(Figs. 3g-i)**, but several osteoclasts could still be identified on the trabecular surfaces. In contrast, ALP-reactivity seemed to be persistent though it slightly tended to be decreased **(Figs 3e-h**, **i)**. Although the index of ALP-reactive area was significantly lower at 1 week, it recovered to be increased at 1 month later, being similar to that of 3 hrs after minodronate administration **(Fig. 3i)**.

Localization of ^{15}N-minodronate assessed by isotope microscope

At three hrs after minodronate administration, most trabecular surfaces showed traces of ^{15}N-minodronate with varying intensities of ^{15}N-minodronate labeling **(Figs. 4a-g)**. After 1 month, ^{15}N-minodronate labeling was seen only on trabeculae that were distant from the growth plate cartilage **(Figs. 4h-n)**. Serial semi-thin sections stained with toluidine blue and isotope microscopic images at 3 hrs after minodronate injection showed a faint ^{15}N-minodronate labeling underneath osteoclasts, while an intense labeling of minodronate was seen adjacent to mature, cuboidal osteoblasts **(Figs. 5a-d)**. The frequency histogram for osteoblast and osteoclast numbers and the ^{15}N/^{14}N intensity ratio demonstrated that most osteoclasts were found on bone surfaces with low ^{15}N/^{14}N ratios, while many osteoblasts were seen on bone surfaces with varying ^{15}N/^{14}N intensity ratios. Thus, the histogram suggests that minodronate seems to be deposited predominantly on bone forming surfaces (beneath osteoblasts) rather than on bone resorbing surfaces (beneath osteoclasts) **(See Figs. 5e and f)**.

High resolution and ultrastructural observation of osteoclasts after minodronate administration

At 3 hrs after minodronate administration, osteoclasts featured the characteristic ruffled border attached to the underlying bone surfaces, while cuboidal, mature osteoblasts were lying on the trabecular surfaces **(Figs. 6a, b)**. However, 24 hrs after minodronate injection, osteoclasts were partially detached from the bone surfaces and had lost their ruffled borders **(Fig. 6c)**. Von Kossa staining showed that osteoclasts not treated with minodronate incorporate fragments of mineralized bone matrix **(Fig. 6d)**, while minodronate-treated osteoclasts failed to do so **(Fig. 6e)**. At one week after minodronate administration, some osteoclasts began to show signs of apoptosis, such as nuclear condensation and spherical cell bodies, while others were still partially attached to the bone surfaces with defective ruffled borders **(Figs. 7a, b)**. TEM images showed osteoclasts with collapsed nuclei and without ruffled borders. On the other hand, these defective osteoclasts extended short cytoplasmic processes towards the bone matrix **(Fig. 7c)**. One month post-injection, the region close to the chondro-osseous junction featured several osteoclasts with well-developed ruffled borders and numerous cuboidal mature osteoblasts on the trabecular surfaces **(Figs. 8a-d)**. Away from the

chondro-osseous junction, most osteoclasts lacked ruffled borders, but there were many mature osteoblasts on the nearby trabeculae **(Fig. 8e, f)**.

Discussion

To our knowledge, this is the first report to show the localization of minodronate *in vivo* in bone tissue. Isotope microscopy demonstrated that ^{15}N-minodronate could be found underneath osteoblasts, *i.e.*, on bone formation surfaces, rather than near bone-resorbing osteoclasts. This finding suggests that the bone-forming trabecular surfaces are coated by minodronate, and we postulated that osteoclasts might somehow fail to resorb the minodronate-coated bone matrix. If osteoclasts do not degrade the minodronate-coated bone matrix, they would not be exposed to minodronate and would not, therefore, enter apoptosis - at least immediately upon administration of the drug. Our histochemical findings demonstrated that many TRAP-positive osteoclasts are seen at all time points studied here, while apoptotic osteoclasts were not clearly identified until the later time points of 1 week and 1 month post-administration. Taken together, a single injection of minodronate seems to produce a long-lasting effect that avoids osteoclastic bone resorption by coating the bone surface and rendering it somewhat “resorption-proof”.

However, this particular tissue distribution seems to produce a “useful” side effect, since maintaining osteoclast presence instead of forcing osteoclastic cells into apoptosis may guarantee osteoblast activation through cell coupling [36]. As shown with the TRAP/ALP double staining, not only TRAP-positive cell numbers were stable, but also many ALP-reactive osteoblasts were persistent even at a later time point (1 month) following minodronate administration, though it temporally decreased at 1 week. Then again, bisphosphonates have been reported to reduce bone formation and bone turnover [12-15]. An autoradiography study showed that alendronate accumulated on resorption surfaces [37], which suggests that alendronate would be readily incorporated by bone-resorbing osteoclasts and immediately halt bone resorption. While alendronate seems to target bone-resorbing osteoclasts directly, minodronate’s distribution and localization on bone formation surfaces indicates that the latter does not inhibit bone-resorbing osteoclasts immediately, but instead protect the bone matrix from osteoclastic bone resorption. In addition, the dysfunctional, non-resorbing osteoclasts may allow nearby osteoblasts somehow to be activated through cell coupling. Retaining osteoblastic activity may favor combined therapy with an anabolic drug such as teriparatide [hPTH(1-34)]. We have demonstrated that cell coupling with osteoclasts

during preosteoblastic differentiation into mature osteoblasts is necessary for parathyroid hormone-driven anabolic effect to occur [38], as others have reported elsewhere [39, 40]. Indeed, daily alendronate administration appears to reduce the anabolic effect of PTH (1-84) on hip bone mineral density (BMD) and cortical volume [41]; on the other hand, combining teriparatide and long-term zoledronate or denosumab treatment produced positive effects on lumbar spine and hip BMD [42, 43]. Likewise, the association of risedronate with teriparatide increased cancellous bone mass in orchidectomized rats [44], as well as lumbar spine, total hip and femoral neck BMD in men [45]. If minodronate sustains osteoblastic activities, as suggested by our findings, it could also produce better results when combined with teriparatide. In fact, one recent study described that a combination of minodronate and teriparatide resulted in increased bone volume and trabecular number, while reducing trabecular separation compared with teriparatide alone [20]. To date, unfortunately, reports focusing on the cumulative effects of once-monthly minodronate and other anabolic drugs are scarce.

In conclusion, minodronate accumulates in bone underneath osteoblasts rather than under bone-resorbing osteoclasts; therefore, it is likely that the minodronate-coated bone matrix is resistant to osteoclastic resorption, which results in a long-lasting and bone-preserving effect.

Conflict of interest

Astellas Pharma Inc., Tokyo, Japan, provided us a ^{15}N- and ^{13}C-labeled minodronate for this study. This study is partially supported by grant from Astellas Pharma Inc., Tokyo, Japan, and grants-in-aid for scientific research and bilateral collaboration (Joint Research Projects and Seminars) of Japan society for the promotion of science, Japan.

AUTHOR CONTRIBUTION STATEMENT

HH and MS: Main researchers contributed equally to this work. Animal experiments, histochemical analysis, observation under isotope microscopy

SK : operating the isotope microscopy

TH and ET: analysis using transmission electron microscopy.

TY and AK: bone histomorphometry and statistical analysis on histological analyses

KT, TN, NK and MA : fixation of animals, extracts femora, decalcification of the specimens, and preparation paraffin sections

KO : providing anti-tissue nonspecific alkaline phosphatase, and working on histogram of the minodronate localization

PF and ML : discussion and preparation of this manuscript, and have been involved in preliminary experiments on the localization of minodronate

HY : Chief of the research center of isotope microscopy, providing experimental protocol on the use of isotope microscopy

NA : Chief of this research project, organizing collaborators and providing a whole idea of this experiment.

All the above authors have read and approved the manuscript prior to submission

References

[1] Russell RGG, Mühlbauer RD, Bisaz S, Williams DA, Fleisch H (1970). The influence of pyrophosphate, condensed phosphates, phosphonates and other phosphate compounds on the dissolution of hydroxyapatitein vitro and on bone resorption induced by parathyroid hormone in tissue culture and in thyroparathyroidectomised rats. Calcif Tissue Res. 6(3): 183-196.

[2] Hansen NM, Felix R, Bisaz S, Fleisch H (1976). Aggregation of hydroxyapatite crystals. Biochim Biophys Acta. 451(2): 549-559.

[3] Francis MD (1969). The inhibition of calcium hydroxyapatite crystal growth by polyphosphonates and polyphosphates. Calcif Tissue Res. 3(2): 151-162.

[4] Hughes DE, Wright KR, Uy HL, Sasaki A, Yoneda T, Roodman GD, Mundy GR, Boyce BF (1995). Bisphosphonates promote apoptosis in murine osteoclasts in vitro and in vivo. J Bone Miner Res. 10(10):1478-1487.

[5] Selander KS, Mönkkönen J, Karhukorpi EK, Härkönen P, Hannuniemi R, Väänänen HK (1996). Characteristics of clodronate-induced apoptosis in osteoclasts and macrophages. Mol Pharmacol. 50(5): 1127-1138.

[6] Amin D, Cornell SA, Gustafson SK, Needle SJ, Ullrich JW, Bilder GE, Perrone MH (1992). Bisphosphonates used for the treatment of bone disorders inhibit squalene synthase and cholesterol biosynthesis. J Lipid Res. 33(11):1657-1663.

[7] Rogers MJ (2003). New insights into the molecular mechanisms of action of bisphosphonates. Curr Pharm Des. 9(32):2643-2658.

[8] Luckman SP, Hughes DE, Coxon FP, Graham R, Russell G Rogers MJ (1998). Nitrogen-containing bisphosphonates inhibit the mevalonate pathway and prevent post-translational prenylation of GTP-binding proteins, including Ras. J Bone Miner Res. 13(11):581-589.

[9] Palokangs H, Mulari M, Vaananen HK (1997). Endocytic pathway from the basal plasma membrane to the ruffled border membrane in bone resorbing osteoclasts. J Cell Sci.

110:1767-1860.

[10] Abu-Amer Y, Teitelbaum SL, Chappel JC, Schlesinger P, Ross FP (1999). Expression and regulation of RAB3 proteins in osteoclasts and their precursors. J Bone Miner Res. 14(11):1855-1860.

[11] Alakangas A, Selander K, Mulari M, Halleen J, Lehenkari P, Mönkkönen J, Salo J, Väänänen K (2002). Alendronate disturbs vesicular trafficking in osteoclasts. Calcif Tissue Int. 70(1):40-47.

[12] Bikle DD, Morey-Holton ER, Doty SB, Currier PA, Tanner SJ, Halloran BP (1994). Alendronate increases skeletal mass of growing rats during unloading by inhibiting resorption of calcified cartilage. J Bone Miner Res. 9(11):1777-1787.

[13] Iwata K, Li J, Follet H, Phipps RJ, Burr DB (2006). Bisphosphonates suppress periosteal osteoblast activity independently of resorption in rat femur and tibia. Bone. 39(5): 1053-1058.

[14] Nakamura M, Udagawa N, Matsuura S, Mogi M, Nakamura H, Horiuchi H, Saito N, Hiraoka BY, Kobayashi Y, Takaoka K, Ozawa H, Miyazawa H, Takahashi N (2003). Osteoprotegerin regulates bone formation through a coupling mechanism with bone resorption. Endocrinology. 144(12): 5441-5449.

[15] Mashiba T, Turner CH, Hirano T, Forwood MR, Johnston CC, Burr DB (2001). Effects of suppressed bone turnover by bisphosphonates on microdamage accumulation and biomechanical properties in clinically relevant skeletal sites in beagles. Bone. 28(5):524-531.

[16] Hagino H, Nishizawa Y, Sone T, Morii H, Taketani Y, Nakamura T, Itabashi A, Mizunuma H, Ohashi Y, Shiraki M, Minamide T, Matsumoto T (2009). A double-blinded head-to-head trial of minodronate and alendronate in women with postmenopausal osteoporosis. Bone. 44(6):1078-1084.

[17] Matsumoto T, Hagino H, Shiraki M, Fukunaga M, Nakano T, Takaoka K, Morii H, Ohashi Y, Nakamura T (2009). Effect of daily oral minodronate on vertebral fractures in Japanese postmenopausal women with established osteoporosis: a randomized placebo-controlled double-blind study. Osteoporos Int. 20(8):1429-1437.

[18] Hagino H, Shiraki M, Fukunaga M, Nakano T, Takaoka K, Ohashi Y, Nakamura T, Matsumoto T (2012). Three years of treatment with minodronate in patients with

postmenopausal osteoporosis. J Bone Miner Metab. 30(4): 439-446.

[19] Yamagami Y, Mashiba T, Iwata K, Tanaka M, Nozaki K, Yamamoto T (2013). Effects of minodronic acid an alendronate on bone remodeling, microdamage accumulation, degree of mineralization and bone mechanical properties in overiectomized cynomolgus monkeys. Bone. 54(1):1-7.

[20] Iwamoto J, Seki A, Sato Y (2014). Effect of combined teriparatide and monthly minodronic acid therapy on cancellous bone mass in ovariectomized rats: A bone histomorphometry study. Bone. 64: 88-94.

[21] Tanaka M, Mori H, Kayasuga R, Ochi Y, Yamada H, Kawada N, Kawabata K (2014). Effect of intermittent and daily regimens of minodronic acid on bone metabolism in an ovariectomized rat model of osteoporosis. Calcif Tissue Int. 95(2):166-173.

[22] Nagira K, Hagino H, Kameyama Y, Teshima R (2013). Effects of minodronate on cortical bone response to mechanical loading rats. Bone. 53(1); 277-283.

[23] Dunford JE, Thompson K, Coxon FP, Luckman SP, Hahn FM, Poulter CD, Ebetino FH, Rogers MJ (2001). Structure-activity relationships for inhibition of farnesyl diphosphate synthase in vitro and inhibition of bone resorption in vivo by nitrogen-containing bisphosphonates. J Pharmacol Exp Ther. 296(2):235-242.

[24] Ebetino FH, Hogan AM, Sun S, Tsoumpra MK, Duan X, Triffitt JT, Kwaasi AA, Dunford JE, Barnett BL, Oppermann U, Lundy MW, Boyde A, Kashemirov BA, McKenna CE, Russell RG (2011). The relationship between the chemistry and biological activity of the bisphosphonates. Bone. 49(1); 20–33.

[25] Confavreux CB, Canoui-Poitrine F, Schott AM, Ambrosi V, Tainturier V, Chapurlat RD (2012). Persistence at 1 year of oral antiosteoporotic drugs: a prospective study in a comprehensive health insurance database. Eur J Endocrinol. 166(4):735–741.

[26] Yurimoto, H., Nagashima, K. and Kunihiro, T (2003). High precision isotope micro-imaging of materials. Appl. Surf. Sci. 203-204, 793-797.

[27] Nagashima K, Krot AN, Yurimoto H (2004). Stardust silicates from primitive meteorites. Nature. 428(6986): 921-924.

[28] Kunihiro T, Nagashima K, Yurimoto H (2005). Microscopic oxygen isotopic homogeneity/heterogeneity in the matrix of the Vigarano CV3 chondrite. Geochim.

Cosmochim. Acta 69: 763-773.

[29] Hamasaki T., Matsumoto T, Sakamoto N, Shimahara A, Kato S, Yoshitake A, Utsunomiya A, Yurimoto H, Gabazza E.C, Ohgi T (2013). Synthesis of ^{18}O-labeled RNA for application to kinetic studies and imaging. Nucleic Acids Research, doi:10.1093/nar/gkt1344.

[30] Kuga Y, Sakamoto N, Yurimoto H (2014). Stable isotope cellular imaging reveals that both live and degenerating fungal pelotons transfer carbon and nitrogen to orchid protocorms. New Phytologist 202: 594-605.

[31] Oda K, Amaya Y, Fukushi-Irie M, Kinameri Y, Ohsuye K, Kubota I, Fujimura S, Kobayashi J (1999). A general method for rapid purification of soluble versions of glycosylphosphatidylinositol-anchored proteins expressed in insect cells: An application for human tissue-nonspecific alkaline phosphatase. J. Biochem. 126(4):694-699.

[32] Amizuka N, Li M, Hara K, Kobayashi M, de Freitas PH, Ubaidus S, Oda K, Akiyama Y (2009). Warfarin administration disrupts the assembly of mineralized nodules in the osteoid.J Electron Microsc. 58(2):55-65.

[33] Sasaki M, Hasegawa T, Yamada T, Hongo H, de Freitas PH, Suzuki R, Yamamoto T, Tabata C, Toyosawa S, Yamamoto T, Oda K, Li M, Inoue N, Amizuka N (2013). Altered distribution of bone matrix proteins and defective bone mineralization in klotho-deficient mice. Bone. 57(1):206-219.

[34] Yamamoto T, Hasegawa T, Sasaki M, Hongo H, Tsuboi K, Shimizu T, Ota M, Haraguchi M, Takahata M, Oda K, Luiz de Freitas PH, Takakura A, Takao-Kawabata R, Isogai Y, Amizuka N (2016). Frequency of teriparatide administration affects the histological pattern of bone formation in young adult male mice. Endocrinology. 157(7):2604-2620.

[35] Parfitt AM, Drezner MK, Glorieux FH, Kanis JA, Malluche H, Meunier PJ, Ott SM, Recker RR (1987). Bone histomorphometry: standardization of nomenclature, symbols, and units. Report of the ASBMR Histomorphometry Nomenclature Committee. J Bone Miner Res 2:595-610.

[36] Frost HM (1969). Tetracycline-based histological analysis of bone remodeling. Calcif Tissue Res. 3:211-237.

[37] Sato M, Grasser W, Endo N, Akins R, Simmons H, Thompson DD, Golub E, Rodan GA (1991). Bisphosphonate action. Alendronate localization in rat bone and effects on

osteoclast ultrastructure. J Clin Invest. 88(6):2095-2105.

[38] Luiz de Freitas PH, Li M, Ninomiya T, Nakamura M, Ubaidus S, Oda K, Udagawa N, Maeda T, Takagi R, Amizuka N (2009). Intermittent PTH administration stimulates pre-osteoblastic proliferation without leading to enhanced bone formation in osteoclast-less c-fos(-/-) mice. J Bone Miner Res. 24(9):1586-1597.

[39] Nishino I, Amizuka N, Ozawa H (2001). Histochemical examination of osteoblastic activity in op/op mice with or without injection of recombinant M-CSF. J Bone Miner Metab. 19(5):267-276.

[40] Sakagami N, Amizuka N, Li M, Takeuchi K, Hoshino M, Nakamura M, Nozawa-Inoue K, Udagawa N, Maeda T (2005). Reduced osteoblastic population and defective mineralization in osteopetrotic (op/op) mice. Micron. 36(7-8):688-695.

[41] Black DM, Greenspan SL, Ensrud KE, Palermo L, McGowan JA, Lang TF, Garnero P, Bouxsein ML, Bilezikian JP, Rosen CJ (2003). The effects of parathyroid hormone and alendronate alone or in combination in postmenopausal osteoporosis.N Engl J Med. 349(13):1207-1215.

[42] Cosman F, Eriksen EF, Recknor C, Miller PD, Guañabens N, Kasperk C, Papanastasiou P, Readie A, Rao H, Gasser JA, Bucci-Rechtweg C, Boonen S (2011). Effects of intravenous zoledronic acid plus subcutaneous teriparatide [rhPTH(1-34)] in postmenopausal osteoporosis.J Bone Miner Res. 26(3):503-511.

[43] Tsai JN, Uihlein AV, Lee H, Kumbhani R, Siwila-Sackman E, McKay EA, Burnett-Bowie SA, Neer RM, Leder BZ (2013). Teriparatide and denosumab, alone or combined, in women with postmenopausal osteoporosis: the DATA study randomised trial. Lancet. 82(9886):50-56.

[44] Iwamoto J, Seki A (2015). Effect of Combined Teriparatide and Monthly Risedronate Therapy on Cancellous Bone Mass in Orchidectomized Rats: A Bone Histomorphometry Study. Calcif Tissue Int. 97(1):23-31.

[45] Walker MD, Cusano NE, Sliney J Jr, Romano M, Zhang C, McMahon DJ, Bilezikian JP (2013). Combination therapy with risedronate and teriparatide in male osteoporosis. Endocrine. 44(1):237-246.

Figure Legends

Fig.1

^{15}N- and ^{13}C-labelled minodronate

As shown here, ^{15}N- and ^{13}C-labelled minodronate [{1-hydroxy-2-[(1-^{15}N)imidazo[1,2-a]pyridin-3-yl](^{13}C2)ethane-1,1-diyl}bis(phosphonic acid) hydrate] was generated by substitution of ^{14}N and ^{12}C in with the stables isotopes ^{15}N and ^{13}C to generate.

Fig. 2

Femoral metaphyseal trabeculae after minodronate administration

Femora treated with single administration of minodronate increased metaphyseal trabeculae as time goes on. Note many trabeculae at 1 week (**c**) and 1 month (**d**) when compared with those at 3 hrs (**a**) and 24 hrs (**b**) after injection. Panels **e**-**h** show highly magnified images of metaphyseal trabeculae. Osteocytes (ocy) seemed intact in all time points (See insets). Panels **i**-**l** show the statistical analyses on bone histomorphometry. Note the significant increases in BV/TV at 1 week and 1 month (**i**) and Tb.N at 1 month (**k**) when compared with those at 3 hrs after the administration, as well as the absence of statistical significance in Tb. Th **(l)**. Tb.Sp. was significantly reduced at 1 week and 1 month after minodronate administration (**j**).

meta: metaphysis

Bars, **a**-**d**: 500μm, **e**-**h**: 100μm

Fig. 3

Double staining of TRAP and ALP on femoral metaphyses after minodronate administration

At all time points, there seemed the distribution of TRAP-positive osteoclasts (red color) and ALP-reactive osteoblasts (brown color) (**a-d**). When observing at a higher magnification, several TRAP-positive osteoclasts were seen throughout the experimental period despite the obvious increase in trabecular volume at 1 week and 1 month post-injection (**e-h**). Please note that apoptotic osteoclasts can be seen at 1 week and 1 month (insets in **g** and **h**). There was no

significant differences in the numbers of TRAP-positive osteoclasts in all the experimental periods (**i**). However, notice apoptotic osteoclasts significantly increased not at the early stage but at the later stage such as 1 week and 1 month of the minodronate injection. Although ALP-reactive area is decreased at 1 week later, it recovered to be increase similar to that at 3 hrs (**j**).
meta: metaphysis, tb: trabecular bone
Bars, **a**-**d**: 200μm, **e**-**h**: 50μm

Fig.4

Localization of ^{15}N-minodronate assessed by isotope microscope

Panels **a**-**g** show the localization of ^{15}N-minodronate at 3 hrs after minodronate administration, while panels **h**-**n** demonstrate ^{15}N-minodronate at 1 month. Panels **a** and **h** show semi-thin sections stained with toluidine blue, which represent the areas of isotope microscopy observation. At 3 hrs, trabecular surfaces showed white lines indicative of ^{15}N-minodronate in all the areas (yellow colored arrows, **b**-**g**). However, after 1 month later, the regions close to the growth plate do not show the labeling of ^{15}N-minodronate, though the distant regions revealed ^{15}N-minodronate (See white lines indicated by yellow arrows in **l**-**n**).
meta: metaphysis, GP: growth plate, dis: diaphysis, bm: bone marrow
Bars, **a**, **h**: 100μm, **b**-**h, i**-**n**: 10μm

Fig.5

Localization of ^{15}N-minodronate on bone-forming surface and bone-resorbing surface

Panels **a**-**d** are serial semi-thin sections stained with toluidine blue (**a**, **c**) and isotope microscopic images (**b**, **d**) at 3 hrs after minodronate injection. Note a faint ^{15}N-minodronate labeling underneath osteoclasts (**a**, **b**), while an intense labeling of minodronate adjacent to mature osteoblasts (**c**, **d**). Panels **e** and **f** are the histogram demonstrating the number of osteoblasts (bone forming surfaces) and osteoclasts (bone resorbing surfaces) located on a regions of varying ^{15}N/^{14}N intensity ratios.
bm: bone marrow
Bars, **a**: 10μm, **b**, **d**: 20μm, **c**: 5μm

Fig. 6

Osteoclasts and osteoblasts at 3hrs and 24 hrs after minodronate administration

Panels **a**-**e** show semi-thin sections stained with toluidine blue. At 3 hrs after minodronate administration, both osteoclasts (oc) and osteoblasts (ob) seem intact: osteoclasts have ruffled

border (RB), while cuboidal, mature osteoblasts were localized on the trabeculae (tb) (**a**, **b**). In contrast, at 24 hrs after minodronate injection, osteoclasts (oc) are shown to be partially detached from the bone surfaces without their ruffled borders (white arrows, **c**). Von Kossa staining visualizes that control osteoclasts (oc) without minodronate treatment incorporate fragments of mineralized bone matrix (brown color, yellow arrows, **d**). However, after minodronate administration, no osteoclasts (oc) are shown to engulf mineralized bone matrices inside (**e**).

BM: mineralized bone matrix

Bars, 10μm

Fig. 7

Osteoclasts at 1 week after minodronate administration

Toluidine blue staining of semi-thin sections (**a**, **b**) showing that some osteoclasts were partially attached to the bone surfaces despite the lack of ruffled borders (an arrow, **a**), and several were apoptotic (double arrows, **b**) at 1 week after minodronate administration. TEM observation demonstrate osteoclasts with collapsed nuclei (an asterisk) and without ruffled borders (See arrowheads, **c**). Such defective osteoclasts extended short cytoplasmic processes towards the bone matrix (BM, arrows, an inset of **c**).

Bars, **a**, **b**: 10μm, **c**: 5μm

Fig. 8

Osteoclasts and osteoblasts at 1 month after minodronate administration

Panels **a**, **b**, **e**, **f** are semi-thin sections stained with toluidine blue, while panels **c** and **d** are TEM images. Panels **a**-**d** are images of osteoclasts (**a**, **c**) and osteoblasts (**b**, **d**) in the close region to the chondro-osseous junction, while panels **e** and **f** are those from the distant region. The region close to the chondro-osseous junction reveals osteoclasts (oc) with well-developed ruffled borders (RB) and numerous cuboidal mature osteoblasts (ob) on the trabeculae when observed under light microscopy (**a**, **b**) and TEM (**c**, **d**). In the distant region from the chondro-osseous junction, most osteoclasts (oc) are fattened, and still lack ruffled borders (**e**), whereas many osteoblasts (ob) are seen (**f**).

Bars, **a, b, e, f**: 10μm, **c**, **d**: 5μm

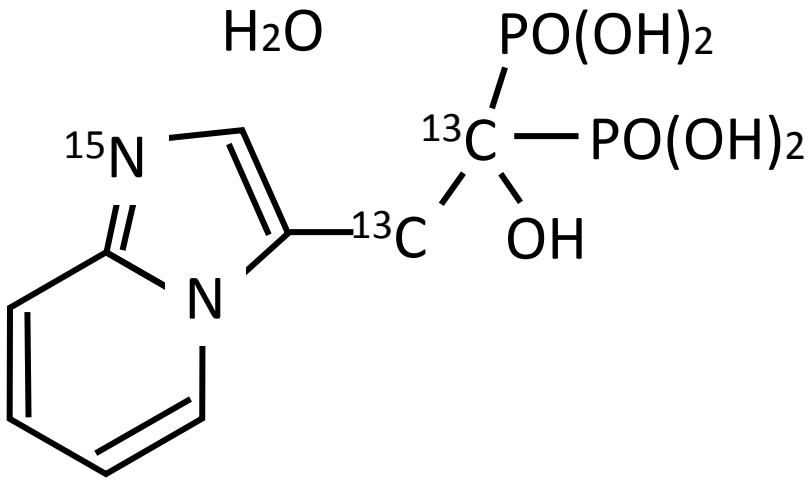

Fig.1

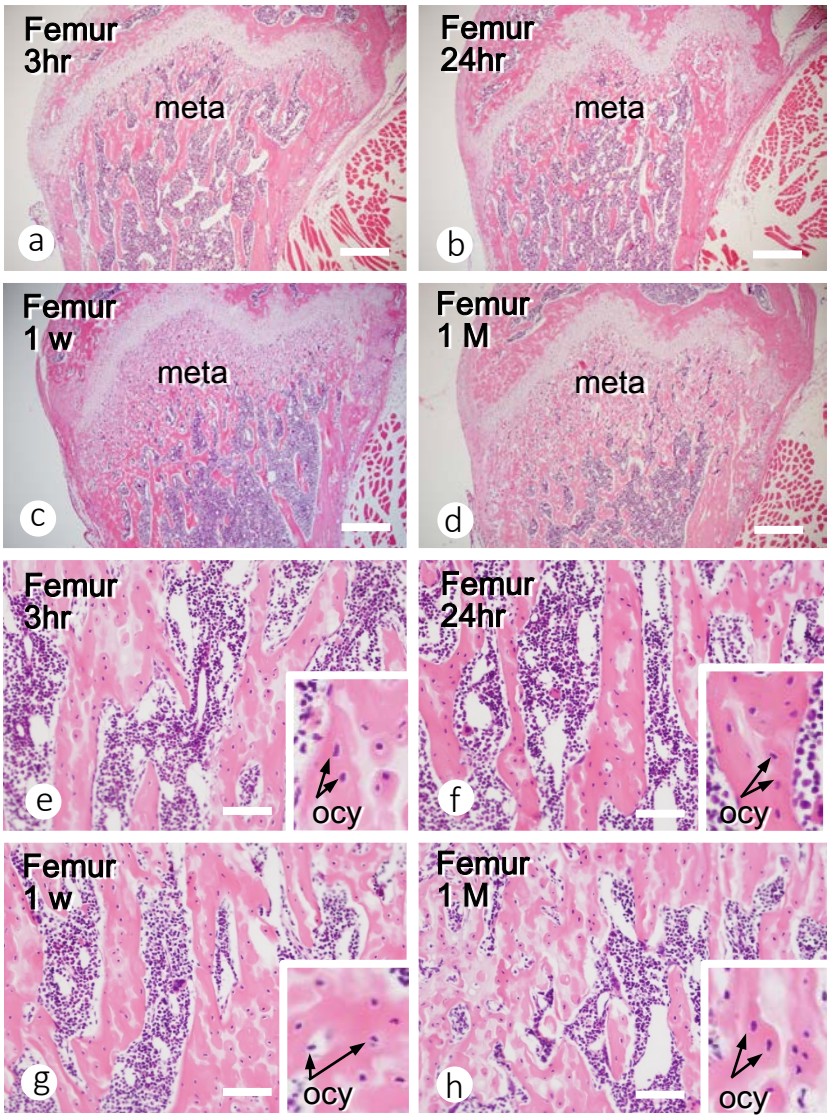
Femur
3hr
meta
a
Femur
24hr
meta
b
Femur
1 w
meta
c
Femur
1 M
meta
d
Femur
3hr
ocy
e
Femur
24hr
ocy
f
Femur
1 w
ocy
g
Femur
1 M
ocy
h

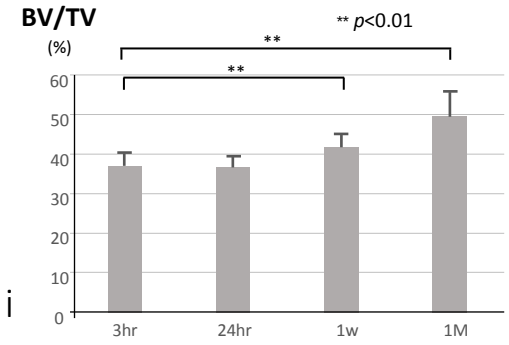
BV/TV
(%)
** p<0.01
**
**
60
50
40
30
20
10
0
3hr
24hr
1w
1M
i

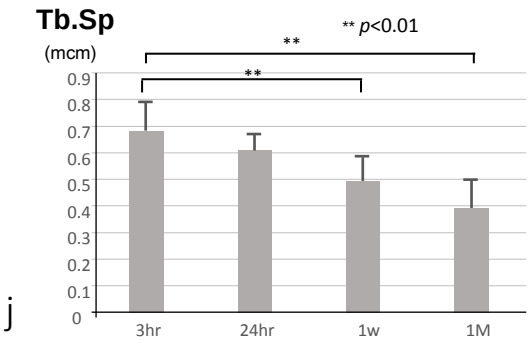
Tb.Sp
(mcm)
** p<0.01
**
**
0.9
0.8
0.7
0.6
0.5
0.4
0.3
0.2
0.1
0
3hr
24hr
1w
1M
j

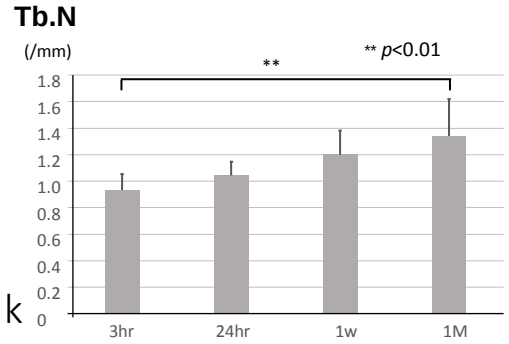
Tb.N
(/mm)
** p<0.01
**
1.8
1.6
1.4
1.2
1.0
0.8
0.6
0.4
0.2
0
3hr
24hr
1w
1M
k

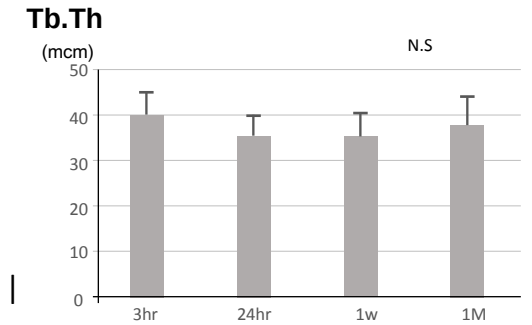
Tb.Th
(mcm)
N.S
50
40
30
20
10
0
3hr
24hr
1w
1M
l

Fig.2

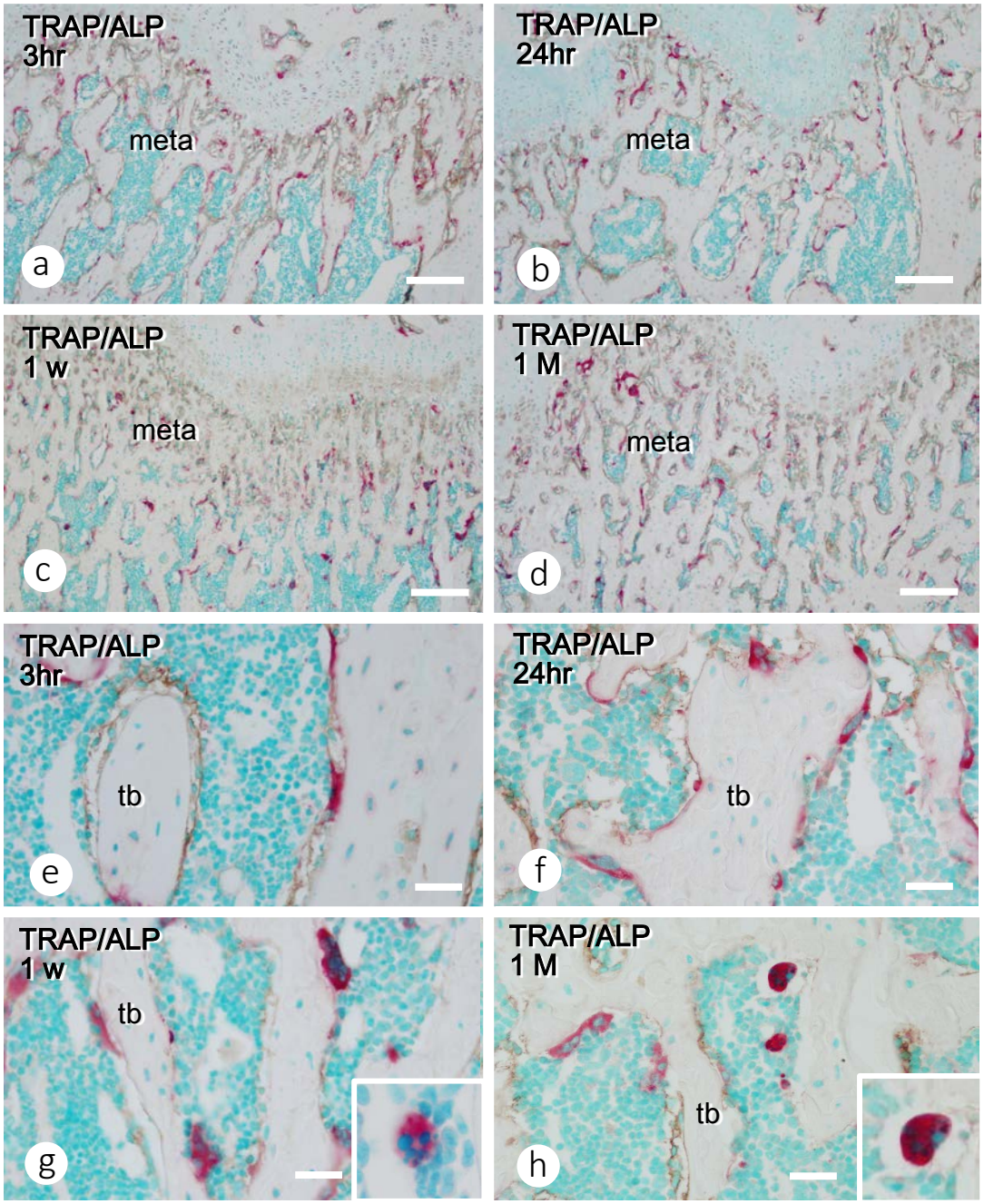

The numbers of TRAP-positive osteoclasts and apoptotic osteoclasts

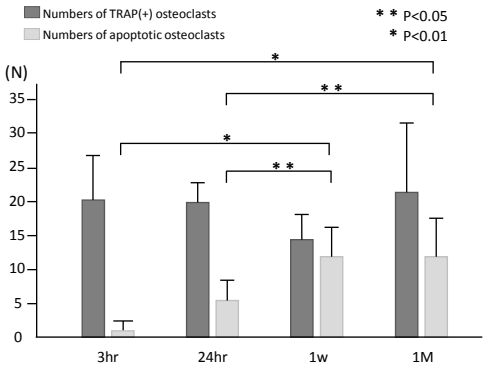

i

ALP reactive area

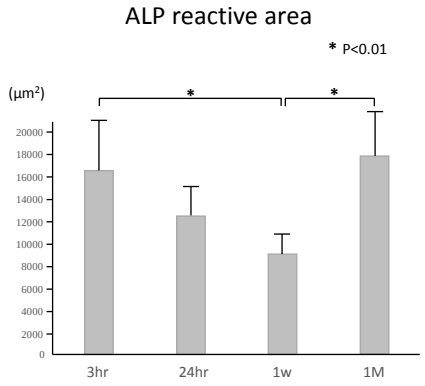

j

Fig.3

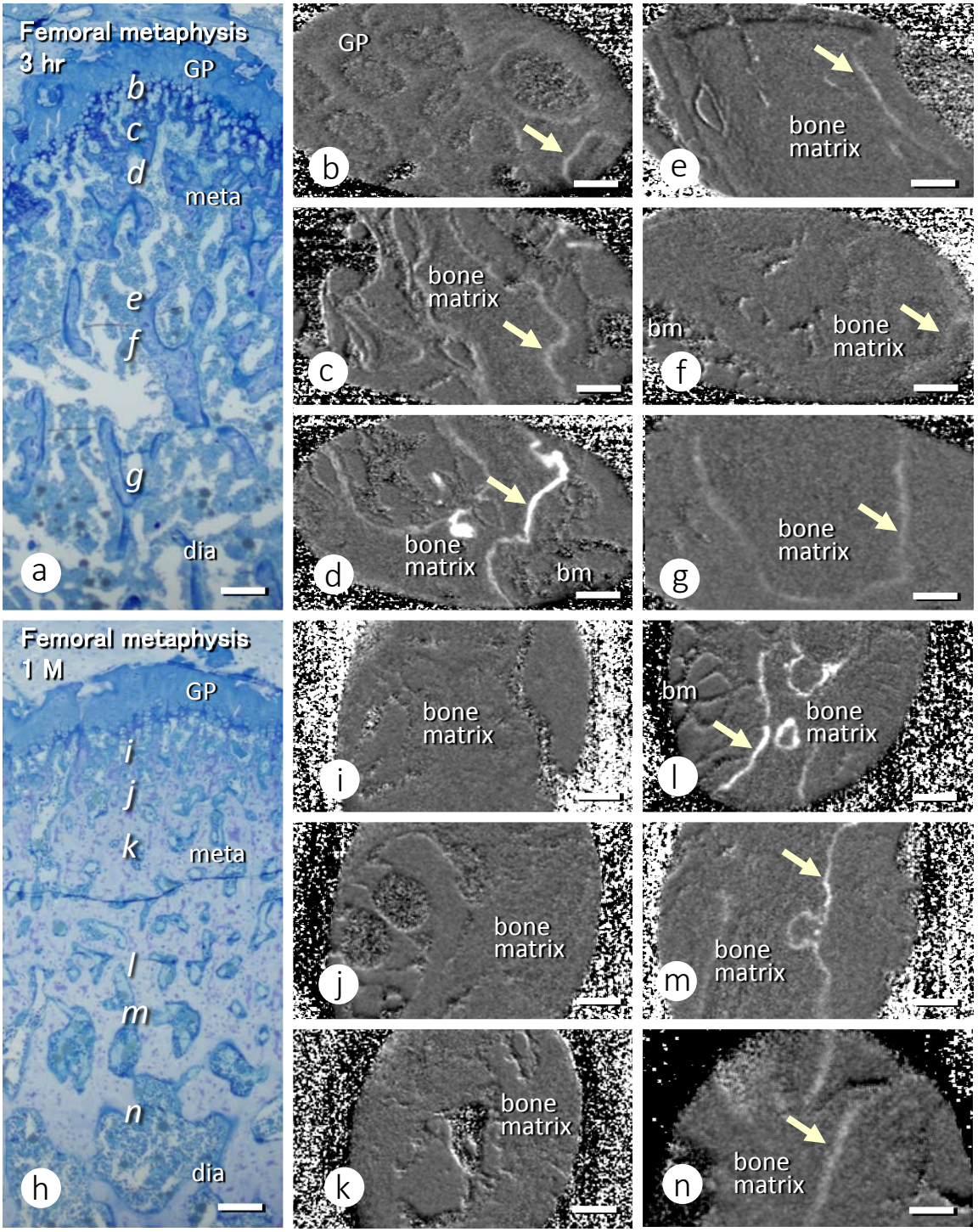
Femoral metaphysis
3 hr
GP
b
c
d
meta
e
f
g
dia
a
GP
b
bone
matrix
c
bone
matrix
d
bone
matrix
bm
e
bone
matrix
f
bm
bone
matrix
g
bone
matrix
Femoral metaphysis
1 M
GP
i
j
k
meta
l
m
n
dia
h
bone
matrix
i
bm
bone
matrix
l
bone
matrix
j
bone
matrix
m
bone
matrix
k
bone
matrix
n

Fig.4

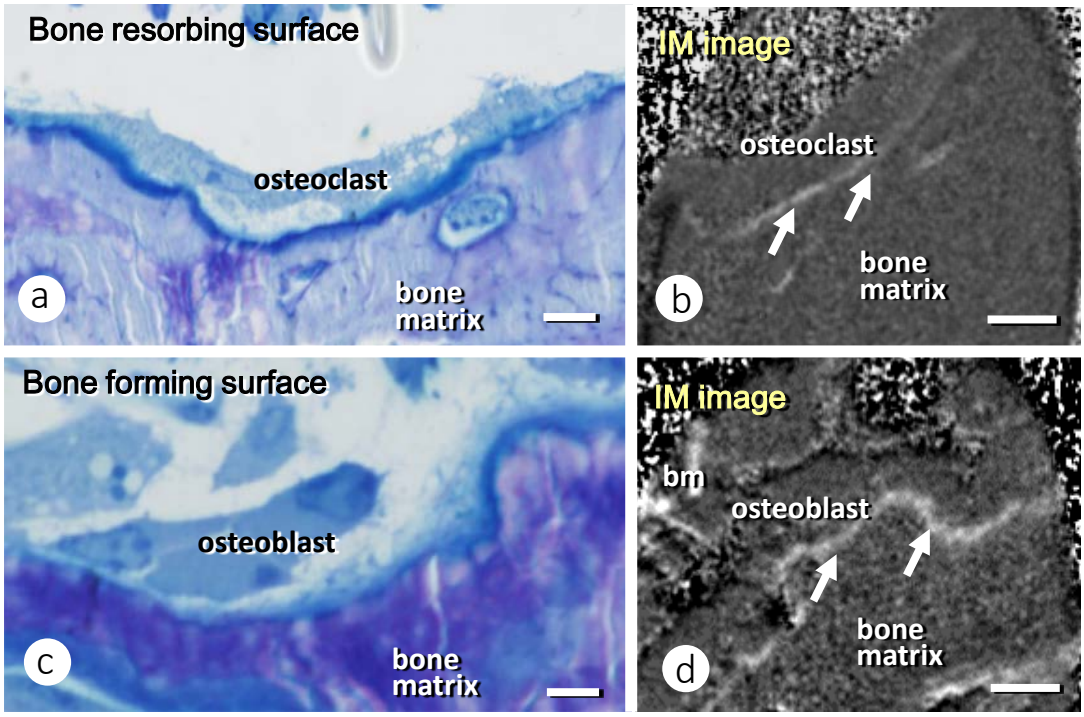
Bone resorbing surface
osteoclast
bone matrix
a
IM image
osteoclast
bone matrix
b
Bone forming surface
osteoblast
bone matrix
c
IM image
bm
osteoblast
bone matrix
d

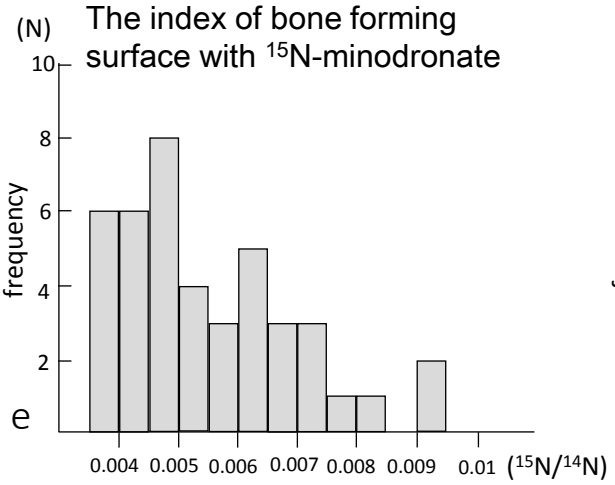
(N)
The index of bone forming surface with ^{15}N-minodronate
frequency
10
8
6
4
2
e
0.004 0.005 0.006 0.007 0.008 0.009 0.01 (^{15}N/^{14}N)

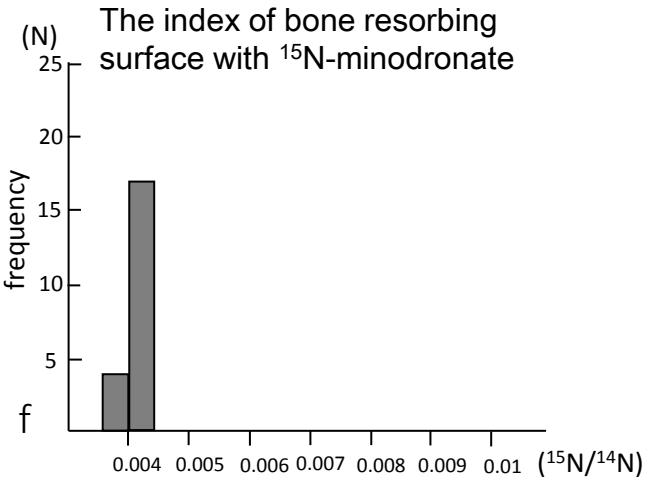
(N)
The index of bone resorbing surface with ^{15}N-minodronate
frequency
25
20
15
10
5
f
0.004 0.005 0.006 0.007 0.008 0.009 0.01 (^{15}N/^{14}N)

Fig.5

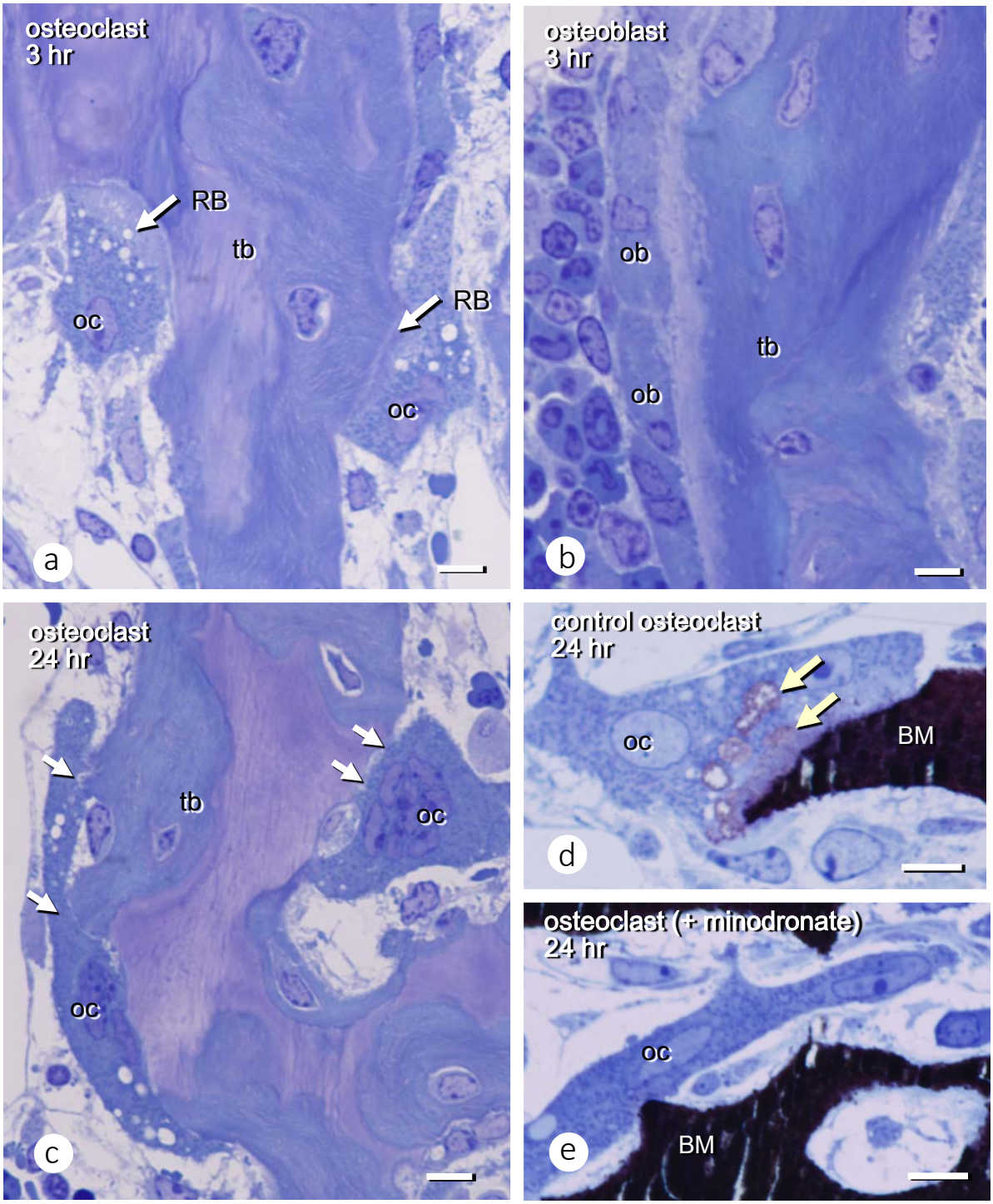
osteoclast
3 hr
RB
tb
RB
oc
oc
a
osteoblast
3 hr
ob
tb
ob
b
osteoclast
24 hr
tb
oc
oc
c
control osteoclast
24 hr
oc
BM
d
osteoclast (+ minodronate)
24 hr
oc
BM
e

Fig.6

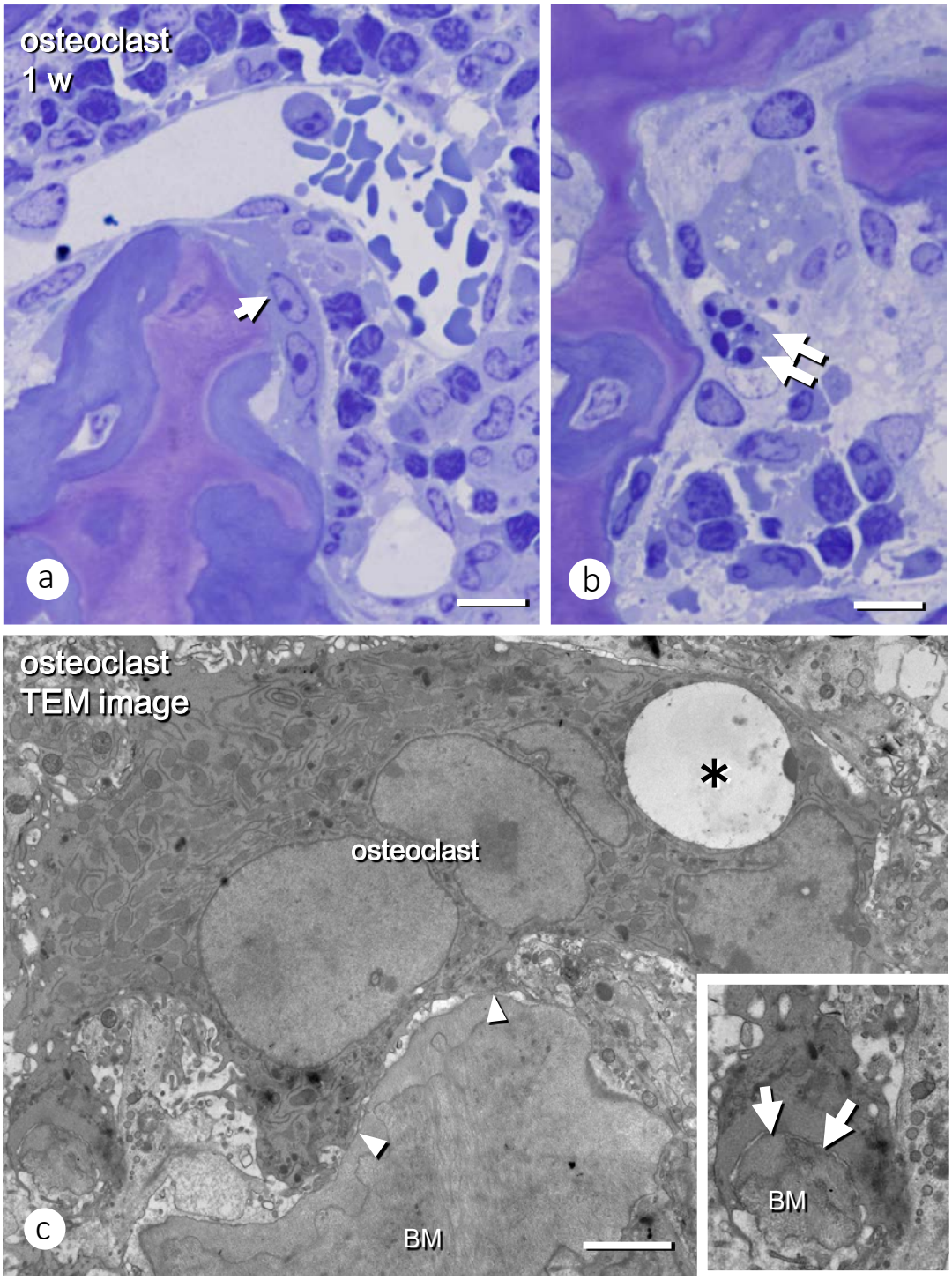

Fig.7

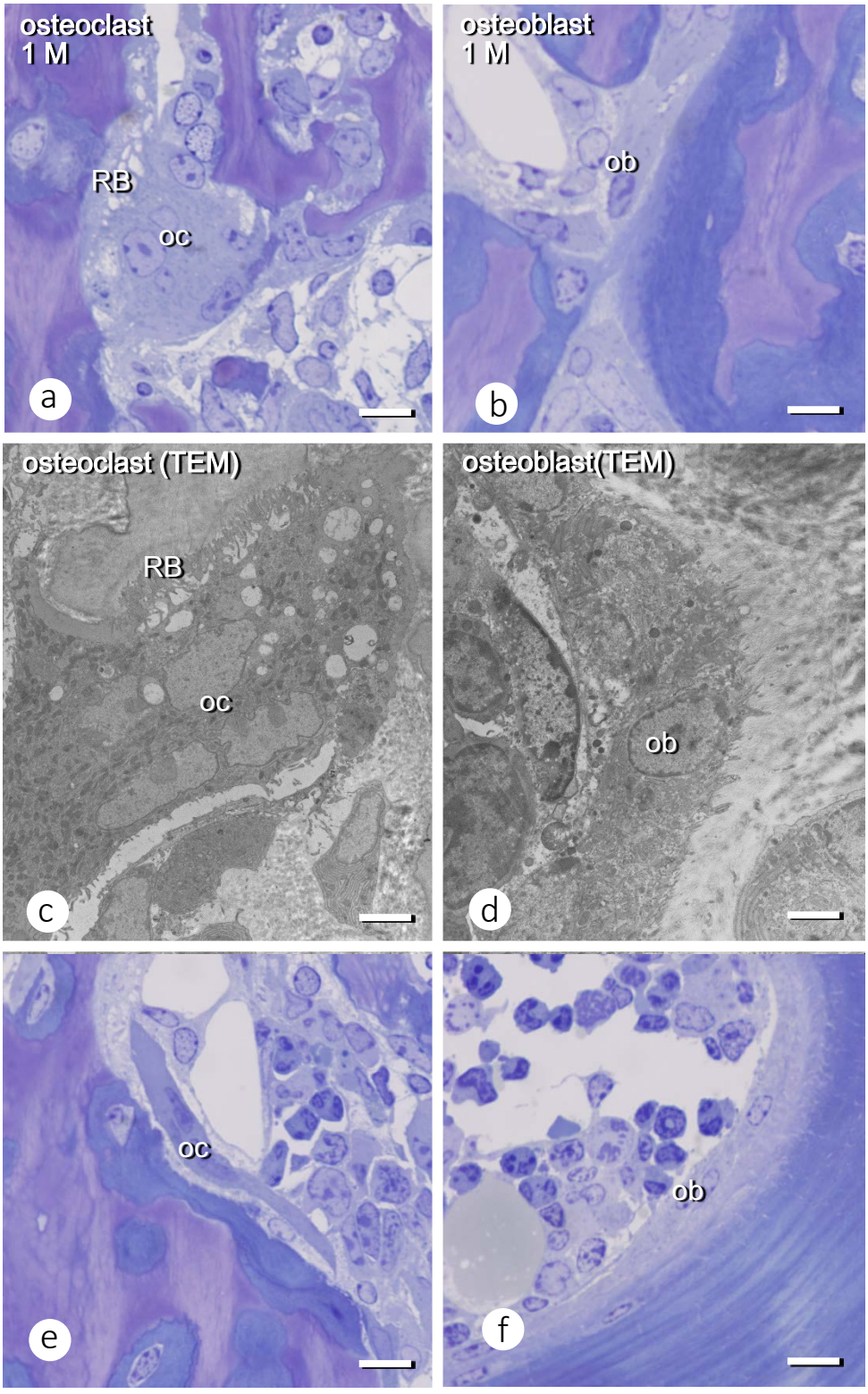
osteoclast
1 M
RB
oc
a
osteoblast
1 M
ob
b
osteoclast (TEM)
RB
oc
c
osteoblast(TEM)
ob
d
oc
e
ob
f

Fig.8